PERGAMON

International Journal of Solids and Structures 37 (2000) 4239–4260

INTERNATIONAL JOURNAL OF SOLIDS and STRUCTURES

www.elsevier.com/locate/ijsolstr

Weak interface in long fiber composites

Stefano Lenci[a, b,*], Giovanni Menditto[a]

[a]*Istituto di Scienza e Tecnica delle Costruzioni, Università di Ancona, via Brecce Bianche, Monte D'Ago, 60131, Ancona, Italy*
[b]*Laboratoire de Modélisation en Mécanique, Université Pierre et Marie Curie (Paris 6), Tour 66, Case 162, 4 Place Jussieu, 75252, Paris, Cedex 05, France*

Received 18 September 1998; in revised form 20 April 1999

Abstract

The problem of the diffusion of load from a fiber to an embedding matrix is considered in a three dimensional context. It is assumed that the fiber-matrix interface allows sliding, which is assumed to be proportional to the interface tangential stress. The close-form solution is obtained for generic loads applied to the fiber, and the case of a concentrated force is studied in detail. The main effects of the interface stiffness, such as avoiding the stress singularities and increasing the length of the zone of influence, are discussed and illustrated by some numerical examples. Successively, the problem of the broken fiber is considered and solved with the same method as the previous case.

Three different situations are discussed: no interaction between fibers, very close neighboring fibers and an intermediate case. It is shown that both problems have the same equations apart from a given function which plays the role of the constitutive equation and which characterizes the considered model. The effect of the neighboring fibers on the interfacial stress is discussed and it is shown that it has a non-monotonic dependence on the distance between the fibers.

Keywords: Elastic interface; Fiber-reinforced composites; Load diffusion; Stress analysis

1. Introduction

The problems related to the diffusion of load from an elastic bar to its surrounding matrix arise in the field of fiber-reinforced composites and in many other branches of engineering. Since the pioneering work of Melan (1932), a great deal of attention has been paid to the determination of interface stresses (Grigolyuk and Tolkachev, 1987), responsible for many characteristic phenomena such as interface delamination, breaking of fibers and so on.

* Corresponding author. Fax: +390-71-220-4576.
E-mail address: m.lenci@fastnet.it (S. Lenci).

0020-7683/00/$ - see front matter
PII: S0020-7683(99)00140-7

Melan has considered two closely related cases. The first consists in the load-transfer problem from an infinite edge-stiffener to a semi-infinite elastic sheet. In the second problem, the string is embedded in an all-around infinite matrix. Koiter (1955) has solved the problem of a semi-infinite fiber glued to an infinite matrix, while Benscoter (1949) has analyzed the same case but with a finite length fiber. The finite length fiber attached to the boundary of a semi-infinite sheet has been considered by Erdogan and Gupta (1971), contrary to Goodier and Hsu (1954) which have studied the case of a fiber normal (and no longer parallel) to the boundary of the semi-infinite matrix.

All the above mentioned works deal with *plane* problems and rely on four basic hypotheses: (i) the sheet is supposed to be in a state of generalized plane stress; (ii) the fiber is regarded as a one-dimensional continuum without stiffness bending; (iii) the bond between bar and sheet is assumed to be perfect (i.e. guaranteeing continuity of stress and displacements); and (iv) it occurs along a (theoretical) line.

Passing to the *three-dimensional* load-transfer problems, the latter hypothesis must be removed because it leads to meaningless integral equations. It is therefore necessary to take into account the actual radius of the fiber, and the possibility of obtaining closed form solutions is strongly reduced. We cite only the solutions given by Muki and Sternberg (1969), which solved the case of a single infinite fiber embedded in an elastic space and loaded by a concentrated force, and by Ford (1973), which considers the case of an infinite broken fiber.

To overcome the previous difficulty, Muki and Sternberg (1969, 1970, 1971) proposed an approximated—though very accurate—model capable of simplifying the mathematical formulation of the problem. Roughly speaking, they regard the original bar as made of two superimposed elastic fibers, the first with the same characteristic as the matrix and treated in the framework of 3D elasticity, the latter with an elastic coefficient equal to the difference between those of the actual fiber and of the matrix, considered as a 1D continuum. The governing integral equation is obtained by imposing the same averaged axial strain in the two fictitious bars.

A more drastic simplification is the well-known *shear lag* model, proposed by Cox (1952), which assumes that the fiber is a 1D medium and that the matrix is subjected only to shear deformations. Although highly approximated, it is currently used to describe several load-transfer problems arising in the applications (Hull, 1981).

More recent contributions are due, for example, to Lee and Mura (1994a, b) and Pak and Saphores (1991), who have obtained the numerical solution in the case of a finite length fiber embedded in elastic space and in elastic half-space.

We have seen that hypotheses (i) and (iv) are naturally removed passing from 2D to 3D. In this paper we relax hypothesis (iii), while hypothesis (ii) seems to be acceptable if one considers the actual dimension of the fibers in practical applications. Our analysis is suggested by the observation of Achenbach and his co-workers (Achenbach and Zhu, 1989, 1990; Choi and Achenbach, 1995) who have noted how in many composites the bond between the fiber and the matrix is not of a perfect kind and allows sliding at the interface, even if continuity of stresses is guaranteed by equilibrium. This interface is called a *weak interface*. The interface is sometimes deliberately weakened by coating the fibers (Peters et al., 1995) or by changing their surface treatment (Subramanian et al., 1996) in order to increase ductility of ceramic matrix composites (Weitsman and Zhu, 1993).

Among the others, a widely used model of the weak interface is the so called 'spring-layer model', which assumes that the jump in displacement is proportional (through constants which characterize the stiffness of the interface) to the interface stress. This model was employed in many situations related to micro-mechanics of composites, e.g. by Lene and Leguillon (1982), Benveniste (1985), Hashin (1990, 1991), Achenbach and Zhu (1989, 1990), Devries (1993). For a theoretical justification and for a more detailed study of the 'spring-layer model' see Geymonat et al. (1999).

This work is devoted to the investigation of the effects of the interface stiffness on the transmission of

load from a fiber to its surrounding matrix. This problem deserves some interest also in certain modern applications of composites in civil engineering. As a matter of fact, there have recently been some attempts to substitute the steel bars for composite bars in concrete. However, as the external peel of the composite bar is made of a thin layer of matrix material, it naturally behaves like a weak interface.

The purpose of this paper is the determination of the stress distribution, in particular the fiber-matrix interface shear stress and the fiber axial force. We have initially studied (section 2) the simplest case of *dilute concentration* (Hashin, 1983), namely, the fibers are far from each other and we can disregard their reciprocal interactions. Therefore, the case of a single fiber embedded in an infinite elastic matrix (Fig. 1) is considered. The solution is obtained for generic loads, and the cases of concentrated force applied to the fiber (section 2.1.) and of broken fiber (section 2.2.) are analyzed in detail because of their relevance in applications.

This problem is preliminary to the more realistic cases where the interactions between the neighboring fibers are taken into account, which are discussed in the following sections 3 and 4. In section 3, we employ the *cylinder model*, which is a reasonable approximation that permits actual computation of the solution. In section 4, on the other hand, the shear lag model is used to determine the effects of neighboring fibers. Section 5 is devoted to the comparison between the different models utilized in this work, while Section 6 contains some conclusions that end the paper.

2. The case of a single fiber embedded in the matrix

In this section, we will consider the case of a single fiber weakly bonded to a surrounding elastic space (Fig. 1). As in Mbanefo and Westmann (1990), we will consider the fiber as a one-dimensional continuum without transversal deformation and we will suppose perfect adherence in the direction

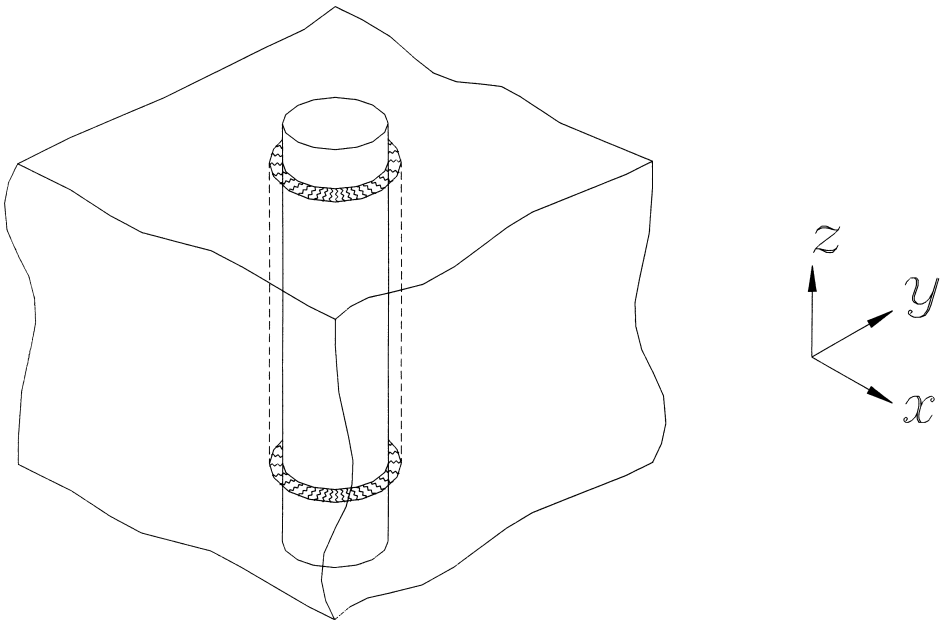

Fig. 1. The dilute concentration problem: a single fiber embedded in an elastic space.

orthogonal to the fiber-matrix interface. In other words, only tangential sliding is allowed for and the normal displacement of the matrix at the interface vanishes.

The matrix material is assumed to be isotropic and linearly elastic, with elastic constants μ and ν. The axial Young modulus of the circular bar and the interface stiffness, on the other hand, are denoted by E and k, respectively. The matrix, the fiber and the interface are homogeneous. In a circular cylindrical coordinate system (r, θ, z), the problem is axially symmetric with respect to the axis of the fiber, which coincides with the z-axis. The axial displacement of the bar is denoted by $U(z)$, the interfacial stress by $\tau(z)$ and the radial and longitudinal displacements of the matrix by $u_r(r, z)$ and $u_z(r, z)$, respectively. We further denote $u(z) = u_z(R, z)$, where R is the radius of the fiber, and we note that the stresses are continuous through the interface (by equilibrium), so that $\tau(z)$ is equal to $\tau_{rz}(R, z)$ and it is the tangential stress applied to the fiber.

As a consequence of the Mbanefo and Westmann hypotheses, at the interface $r = R$ we have

$$u_r(R, z) = 0, \quad \forall z \in]-\infty, \infty[, \tag{1a}$$

$$\tau(z) = k[u(z) - U(z)], \quad \forall z \in]-\infty, \infty[. \tag{1b}$$

Taking the Fourier transform $\hat{f}(s) = \int_{-\infty}^{\infty} f(z) e^{isz}\, dz$ (Sneddon, 1951) of (1) we obtain

$$\hat{u}_r(R, s) = 0, \quad \forall s \in]-\infty, \infty[, \tag{2a}$$

$$\hat{\tau}(s) = k[\hat{u}(s) - \hat{U}(s)], \quad \forall s \in]-\infty, \infty[. \tag{2b}$$

The non-vanishing stresses and displacements in the matrix can be expressed in terms of the Love potential (Love, 1926, art. 188) as follows:

$$u_r(r, z) = -\frac{\partial^2 \phi}{\partial r \partial z}, \tag{3a}$$

$$u_z(r, z) = 2(1 - \nu)\nabla^2 \phi - \frac{\partial^2 \phi}{\partial z^2}, \tag{3b}$$

$$\tau_{rr}(r, z) = 2\mu \frac{\partial}{\partial z}\left[\nu \nabla^2 \phi - \frac{\partial^2 \phi}{\partial r^2}\right], \tag{3c}$$

$$\tau_{\theta\theta}(r, z) = 2\mu \frac{\partial}{\partial z}\left[\nu \nabla^2 \phi - \frac{1}{r}\frac{\partial \phi}{\partial r}\right], \tag{3d}$$

$$\tau_{zz}(r, z) = 2\mu \frac{\partial}{\partial z}\left[(2 - \nu)\nabla^2 \phi - \frac{\partial^2 \phi}{\partial z^2}\right], \tag{3e}$$

$$\tau_{rz}(r, z) = 2\mu \frac{\partial}{\partial r}\left[(1 - \nu)\nabla^2 \phi - \frac{\partial^2 \phi}{\partial z^2}\right], \tag{3f}$$

where

$$\nabla^2 = \frac{\partial^2}{\partial r^2} + \frac{1}{r}\frac{\partial}{\partial r} + \frac{\partial^2}{\partial z^2}$$

is the axisymmetric Laplacian operator. In the absence of body force, the function $\phi(r, z)$ is biharmonic, i.e. $\nabla^2\nabla^2\phi = 0$, in its domain $(r, z) =]R,\infty[\times]-\infty,\infty[$. The Fourier transforms of Eq. (3) are

$$\hat{u}_r(r, s) = is\frac{\partial\hat{\phi}}{\partial r}, \tag{4a}$$

$$\hat{u}_z(r, s) = 2(1-v)\hat{\nabla}^2\hat{\phi} + s^2\hat{\phi}, \tag{4b}$$

$$\hat{\tau}_{rr}(r, s) = -2\mu is\left[v\hat{\nabla}^2\hat{\phi} - \frac{\partial^2\hat{\phi}}{\partial r^2}\right], \tag{4c}$$

$$\hat{\tau}_{\theta\theta}(r, s) = -2\mu is\left[v\hat{\nabla}^2\hat{\phi} - \frac{1}{r}\frac{\partial\hat{\phi}}{\partial r}\right], \tag{4d}$$

$$\hat{\tau}_{zz}(r, s) = -2\mu is[(2-v)\hat{\nabla}^2\hat{\phi} + s^2\hat{\phi}], \tag{4e}$$

$$\hat{\tau}_{rz}(r, s) = 2\mu\frac{\partial}{\partial r}[(1-v)\hat{\nabla}^2\hat{\phi} + s^2\hat{\phi}], \tag{4f}$$

where

$$\hat{\nabla}^2 = \frac{\partial^2}{\partial r^2} + \frac{1}{r}\frac{\partial}{\partial r} - s^2.$$

The function $\hat{\phi}(r, s)$ satisfies $\hat{\nabla}^2\hat{\nabla}^2\hat{\phi} = 0$ on $(r, s) =]R, \infty[\times]-\infty, \infty[$. The general solution of this equation is

$$\hat{\phi}(r, s) = A(s)K_0(|s|r) + B(s)|s|rK_1(|s|r) + C(s)I_0(|s|r) + D(s)|s|rI_1(|s|r), \tag{5}$$

where K_n and I_n are the nth-order modified Bessel functions (Abramowitz and Stegun, 1970, section 9). The condition of bounded stress for $r \to \infty$ implies $C(s) = D(s) = 0$, $\forall s\in]-\infty, \infty[$, while from Eq. (1a) it follows

$$A(s) = -\frac{|s|RK_0(|s|R)}{K_1(|s|R)}B(s), \tag{6}$$

which gives the unknown stresses and displacements in terms of $B(s)$. The substitution of Eq. (6) in (5) and (4) gives, in particular,

$$\hat{\tau}(s) = \hat{\tau}_{rz}(R, s) = B(s)4\mu(1-v)|s|^3 K_1(|s|R), \tag{7a}$$

$$\hat{u}(s) = \hat{u}_z(R, s) = B(s)s^2K_0(|s|R)\left[-4(1-v) - \frac{|s|RK_0(|s|R)}{K_1(|s|R)} + \frac{|s|RK_1(|s|R)}{K_0(|s|R)}\right], \tag{7b}$$

from which

$$\hat{u}(s) = \hat{\tau}(s)\frac{R}{\mu}g(|\, s \,|\, R), \tag{8}$$

where

$$g(x) = -\frac{1}{x}\frac{K_0(x)}{K_1(x)} - \frac{1}{4(1-\nu)}\left(\frac{K_0(x)}{K_1(x)}\right)^2 + \frac{1}{4(1-\nu)}, \quad x > 0. \tag{9}$$

As we will see in the sequel, the function $g(x)$, which relates the Fourier transforms of the stress and displacement of the matrix at the interface, plays a central role in obtaining the solutions of different problems on the basis of the solution obtained in this section. Therefore, in some sense, it characterizes the model of fiber reinforcement we are considering.

To obtain the solution of the problem, it remains to consider the equilibrium equation of the bar

$$\frac{\mathrm{d}^2U(z)}{\mathrm{d}z^2} + \frac{2}{ER}\tau(z) - \frac{\mathrm{d}\epsilon^*(z)}{\mathrm{d}z} + \frac{f(z)}{E} = 0, \quad \forall z \in]-\infty, \infty[, \tag{10}$$

where $f(z)$ and $\epsilon^*(z)$ are the applied body-force density (per unit volume) and the imposed axial strain (for example, the strain due to the increase of the temperature), respectively. On applying the Fourier transform to Eq. (10), one arrives at

$$-s^2\hat{U}(s) + \frac{2}{ER}\hat{\tau}(s) + is\hat{\epsilon}^*(s) + \frac{1}{E}\hat{f}(s) = 0, \quad \forall s \in]-\infty, \infty[. \tag{11}$$

Summarizing, the resolvent system is given by Eqs. (2b), (8) and (11), namely,

$$\begin{bmatrix} 1 & -k & +k \\ -g(|\, s \,|\, R)(R/\mu) & 1 & 0 \\ -2/(ER) & 0 & s^2 \end{bmatrix}\begin{bmatrix} \hat{\tau}(s) \\ \hat{u}(s) \\ \hat{U}(s) \end{bmatrix} = \begin{bmatrix} 0 \\ 0 \\ is\hat{\epsilon}^*(s) + \hat{f}(s)/E \end{bmatrix} \tag{12}$$

from which

$$\hat{\tau}(s) = -\frac{i\xi E\hat{\epsilon}^*(\xi/R) + R\hat{f}(\xi/R)}{\frac{E}{kR}\xi^2 - \frac{E}{\mu}\xi^2 g(|\, \xi \,|) + 2}, \tag{13a}$$

$$\hat{u}(s) = -\frac{R}{\mu}g(|\, \xi \,|)\frac{i\xi E\hat{\epsilon}^*(\xi/R) + R\hat{f}(\xi/R)}{\frac{E}{kR}\xi^2 - \frac{E}{\mu}\xi^2 g(|\, \xi \,|) + 2}, \tag{13b}$$

$$\hat{U}(s) = \left(\frac{1}{k} - \frac{R}{\mu}g(|\, \xi \,|)\right)\frac{i\xi E\hat{\epsilon}^*(\xi/R) + R\hat{f}(\xi/R)}{\frac{E}{kR}\xi^2 - \frac{E}{\mu}\xi^2 g(|\, \xi \,|) + 2}, \tag{13c}$$

where $\xi = Rs$. For later use, we also define $\zeta = z/R$. The inverse Fourier transforms $f(z) = (2\pi)^{-1}\int_{-\infty}^{\infty}\hat{f}(s)\mathrm{e}^{-\mathrm{i}sz}\,\mathrm{d}s$ (Sneddon, 1951) of Eq. (13) give the solution of the problem for every $f(z)$ and $\epsilon^*(z)$.

We report the expressions of $\hat{\tau}_{rr}(R, s)$ and $\hat{\tau}_{zz}(R, s)$, which are directly concerned with the problems of resistance of the fiber-reinforced composites. In fact, the possibility of normal debonding depends on the

magnitude of the normal stress at the interface, which can be computed by inverting its Fourier transform, given by

$$\hat{\tau}_{rr}(R, s) = -i\left(2\xi g(|\xi|) + \mathrm{sign}(\xi)\frac{K_0(|\xi|)}{K_1(|\xi|)}\right)\frac{i\xi E\hat{\epsilon}^*(\xi/R) + R\hat{f}(\xi/R)}{\frac{E}{kR}\xi^2 - \frac{E}{\mu}\xi^2 g(|\xi|) + 2}. \tag{14}$$

The failure of the matrix, on the other hand, strongly depends on the normal stress in the z direction at $r = R$. By using Eqs. (4) and (13), its Fourier transform can be expressed in the form

$$\hat{\tau}_{zz}(R, s) = 2i\xi\left(g(|\xi|) - \frac{v}{2(1-v)}\,\frac{1}{|\xi|}\,\frac{K_0(|\xi|)}{K_1(|\xi|)}\right)\frac{i\xi E\hat{\epsilon}^*(\xi/R) + R\hat{f}(\xi/R)}{\frac{E}{kR}\xi^2 - \frac{E}{\mu}\xi^2 g(|\xi|) + 2}. \tag{15}$$

2.1. The concentrated force applied to the fiber

When the fiber is loaded by a concentrated force applied at $z = 0$, we have $\hat{f}(s) = P/(\pi R^2)$ and $\hat{\epsilon}^*(s) = 0$. In these circumstances Eqs. (13)–(15) supply, after some simplifications,

$$\tau(\zeta) = -\frac{P}{\pi^2 R^2}\int_0^\infty \frac{\cos(\xi\zeta)}{\frac{E}{kR}\xi^2 - \frac{E}{\mu}\xi^2 g(\xi) + 2}\,\mathrm{d}\xi, \tag{16a}$$

$$u(\zeta) = -\frac{P}{\mu\pi^2 R}\int_0^\infty \frac{g(\xi)\cos(\xi\zeta)}{\frac{E}{kR}\xi^2 - \frac{E}{\mu}\xi^2 g(\xi) + 2}\,\mathrm{d}\xi, \tag{16b}$$

$$U(\zeta) = -\frac{P}{E\pi^2 R}\int_0^\infty \left[\frac{E}{kR} - \frac{E}{\mu}g(\xi)\right]\frac{\cos(\xi\zeta)}{\frac{E}{kR}\xi^2 - \frac{E}{\mu}\xi^2 g(\xi) + 2}\,\mathrm{d}\xi, \tag{16c}$$

$$\tau_{rr}(\zeta) = -\frac{P}{\pi^2 R^2}\int_0^\infty \left[2\xi g(\xi) + \frac{K_0(\xi)}{K_1(\xi)}\right]\frac{\sin(\xi\zeta)}{\frac{E}{kR}\xi^2 - \frac{E}{\mu}\xi^2 g(\xi) + 2}\,\mathrm{d}\xi, \tag{16d}$$

$$\tau_{zz}(\zeta) = \frac{P}{\pi^2 R^2}\int_0^\infty \left[2\xi g(\xi) - \frac{v}{1-v}\,\frac{K_0(\xi)}{K_1(\xi)}\right]\frac{\sin(\xi\zeta)}{\frac{E}{kR}\xi^2 - \frac{E}{\mu}\xi^2 g(\xi) + 2}\,\mathrm{d}\xi. \tag{16e}$$

It is possible to show that the integrals (16a–c) are absolutely and uniformly convergent. Focusing on $\tau(\zeta)$, this implies that the interfacial stress is Lipschitz-continuous. Furthermore, $\tau(\zeta)$ is bounded everywhere and $|\tau(\zeta)| < \tau_{\max} = |\tau(0)|$. The boundedness is lost when $k \to +\infty$, because the interfacial stress becomes (logarithmically) unbounded for $\zeta \to 0$, as is also shown, in a slightly different model, by Muki and Sternberg (1969).

The previous discussions show that the weak interface avoids the interface stress singularities. This property may be used in practice to prevent interfacial debonding, and in some cases k can be utilized as

a design parameter to optimize the mechanical properties of the composite. For example, it is sufficient to choose the interfacial stiffness k in such a way that τ_{max} is lower than its failure value. In this respect, an important role is played by the function $\tau_{max}=\tau_{max}(k)$, which is given by

$$\tau_{max}(k)=\frac{P}{\pi^2R^2}\int_0^{\infty}\frac{d\xi}{\frac{E}{kR}\xi^2-\frac{E}{\mu}\xi^2 g(\xi)+2}, \tag{17}$$

and which is drawn in Fig. 2 for a glass-epoxy composite (in this case the elastic modulus of the fiber is $E = 68.954$ GPa, while the matrix is characterized by $\nu=0.34$ and $\mu=2.59$ GPa (Tandon, 1995), so that $E/\mu=26.62$. These values will be employed in *all* the following numerical examples). Note that, according to the previous discussions, $\tau_{max}(k)$ tends to infinity as $k\to+\infty$. For the same materials, we have reported in Fig. 3 the interface tangential stress $\tau(\zeta)$. This function is always negative, strictly increasing for $\zeta > 0$ and vanishing for $|\zeta|\to\infty$. When k is high, the solution has a peak in a neighborhood of the force application point, while in the opposite case it is spread on the 'whole' interface.

The radial and longitudinal stresses in the matrix at the interface (see Eq. (16d and e)) are depicted in Figs. 4 and 5, respectively. For every value of k, they are initially increasing (in absolute value), they reach a maximum at, say, $\hat{\zeta}=\hat{\zeta}(k)>0$ and then they tend to zero far from the force application point. Again, for high values of interface stiffness the stresses are 'concentrated' around $\zeta=0$, while they are spread when k is low.

Figs. 4 and 5 show that $\tau_{rr}(\zeta)$ is one order of magnitude lower than $\tau_{zz}(\zeta)$ and $\tau(\zeta)$. This suggests that, except for the special cases of interfaces with very low normal resistance, the damage mechanism of normal debonding at the interface should not occur in the present case. The other aspect emphasized by Figs. 4 and 5 is that the maximum normal stresses are not attained at $\zeta=0$, as in the case $k\to\infty$, but rather for a given $\hat{\zeta}>0$ depending on k. Thus, one effect of the weak interface is that possible failure of the matrix may start at points different from the force application point. This observation is based on qualitative reasoning, but can be stated rigorously introducing failure criteria for the matrix. This analysis, however, is not within the scopes of the present paper.

The axial force in the bar is obtained by the constitutive relation $N(\zeta)=E\pi R(dU/d\zeta)$, and therefore it is given by

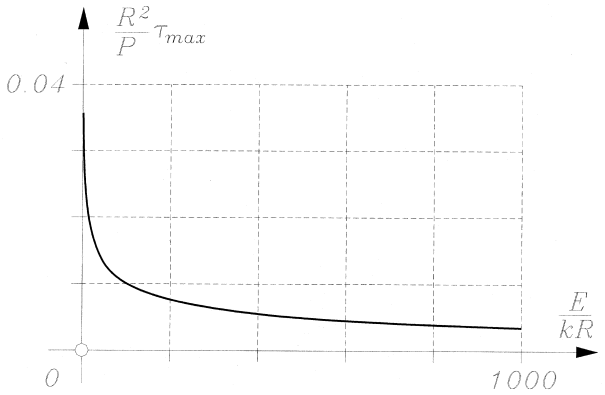

Fig. 2. The function $\tau_{max}(k)$.

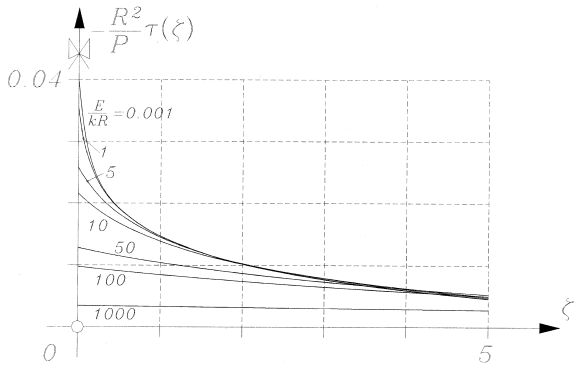

Fig. 3. The function $\tau(\zeta)$ for different values of the interface stiffness.

$$N(\zeta)=\frac{P}{2}\left\{-\operatorname{sign}(\zeta)+\frac{4}{\pi}\int_0^\infty \frac{\sin(\xi\zeta)}{\dfrac{E}{kR}\xi^3-\dfrac{E}{\mu}\xi^3 g(\xi)+2\xi}\,\mathrm{d}\xi\right\}. \tag{18}$$

In absolute value, it ranges from $P/2$ (for $\zeta=0$) to zero (for $|\zeta|\to\infty$) (Fig. 6). It follows that at a certain distance from $\zeta=0$ the effects of the applied load become negligible. We define the (nominal) length of the *zone of influence* the segment for which the axial load is greater than 5% of the applied force. Thus, the semi-length $\bar{\zeta}$ is obtained by solving $N(\bar{\zeta})=0.05P$. The numerical solution of this equation for the glass-epoxy composite is depicted in Fig. 7(a). As expected, the length of the zone of influence is inversely proportional to the interface stiffness.

2.2. The broken fiber

In polymeric fiber-reinforced composites, the external load is carried almost entirely by the fibers, and it is very common that they break, usually as a consequence of some extra load due to unavoidable imperfections. When one fiber breaks, however, its axial force is transferred to the matrix, which increases its stress and which may fail if there is no extra resistance. Thus, it is of practical interest to study the extra-stress induced in the matrix as a consequence of the breaking of fibers. This problem is

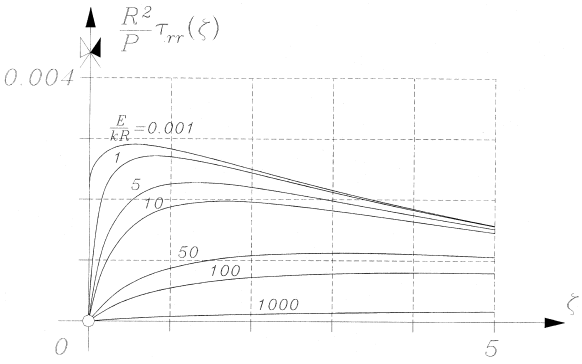

Fig. 4. The function $\tau_{rr}(\zeta)$ for different values of the interface stiffness.

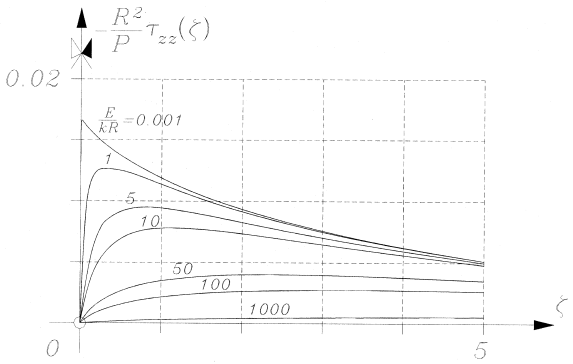

Fig. 5. The function $\tau_{zz}(\zeta)$ for different values of the interface stiffness.

dealt with in this section, where we consider the case of a single broken fiber embedded in the matrix. The interaction with the unbroken neighboring fibers will be analyzed in the next sections.

As in (Mbanefo and Westmann, 1990), we suppose that the matrix is loaded by a given constant strain $\epsilon_{zz}=\tilde{\epsilon}$ at infinity. Using the linearity of the problem, however, we can consider the case of the fiber subjected to a concentrated jump of displacement $\Delta = U(0^+) - U(0^-) > 0$ with vanishing strains (and stresses) at infinity. This gives a non-zero compressive force $N(0^+) = N(0^-) = -N(\Delta)$. To obtain the solution in terms of the actual applied strain $\tilde{\epsilon}$, it is then sufficient to equate $N(\Delta)$ with $\tilde{\epsilon}E\pi R^2$ (the axial force in the uniform case), obtaining $\Delta = \Delta(\tilde{\epsilon})$, and adding to this solution the constant strain solution.

In the present case we have $\hat{f}(s)=0$, $\hat{\epsilon}^*(s)=\Delta$, and inverting Eqs. (13)–(15) we obtain

$$\tau(\zeta) = -\frac{k\Delta}{2}\left\{\operatorname{sign}(\zeta) - \frac{2}{\pi}\int_0^\infty \left[-\frac{E}{\mu}\xi^2 g(\xi)+2\right]\frac{\sin(\xi\zeta)}{\dfrac{E}{kR}\xi^3 - \dfrac{E}{\mu}\xi^3 g(\xi)+2\xi}\,\mathrm{d}\xi\right\}, \tag{19a}$$

$$u(\zeta) = \frac{\Delta}{\pi}\int_0^\infty \left[-\frac{E}{\mu}g(\xi)\xi\right]\frac{\sin(\xi\zeta)}{\dfrac{E}{kR}\xi^2 - \dfrac{E}{\mu}\xi^2 g(\xi)+2}\,\mathrm{d}\xi, \tag{19b}$$

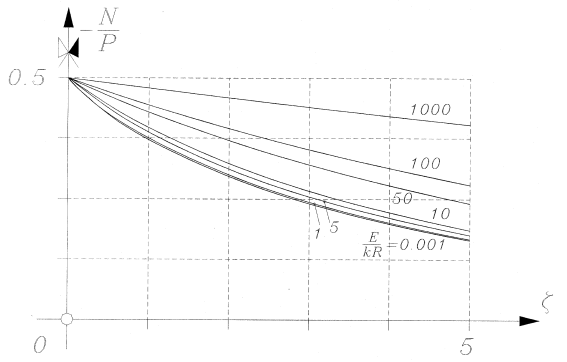

Fig. 6. The axial load in the fiber for different values of the interface stiffness.

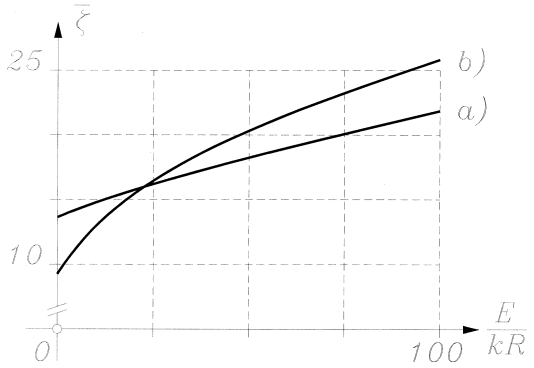

Fig. 7. The semi-length of the zone of influence versus the interface stiffness in the case (a) of concentrated force (section 2.1.) and (b) of broken fiber (section 2.2.).

$$U(\zeta) = \frac{\Delta}{2}\left\{\operatorname{sign}(\zeta) - \frac{4}{\pi}\int_0^\infty \frac{\sin(\xi\zeta)}{\dfrac{E}{kR}\xi^3 - \dfrac{E}{\mu}\xi^3 g(\xi) + 2\xi}\,\mathrm{d}\xi\right\}, \tag{19c}$$

$$\tau_{rr}(\zeta) = \frac{\Delta E}{\pi R}\int_0^\infty \left[2\xi^2 g(\xi) + \xi\frac{K_0(\xi)}{K_1(\xi)}\right]\frac{\cos(\xi\zeta)}{\dfrac{E}{kR}\xi^2 - \dfrac{E}{\mu}\xi^2 g(\xi) + 2}\,\mathrm{d}\xi, \tag{19d}$$

$$\tau_{zz}(\zeta) = -\frac{\Delta E}{\pi R}\int_0^\infty \left[2\xi^2 g(\xi) - \frac{\nu}{1-\nu}\xi\frac{K_0(\xi)}{K_1(\xi)}\right]\frac{\cos(\xi\zeta)}{\dfrac{E}{kR}\xi^2 - \dfrac{E}{\mu}\xi^2 g(\xi) + 2}\,\mathrm{d}\xi. \tag{19e}$$

The interface tangential stress, which is depicted in Fig. 8 for the glass-epoxy composite, is, for $\zeta > 0$, negative, increasing, with minimum $\tau(0) = -k\Delta/2$ and vanishes for $\zeta \to \infty$. Furthermore, when the interface is very soft (low values of k), the interface tangential stress is 'almost' constant, while it rapidly decreases to zero in the case of very stiff interfaces.

Remark. The problems treated in sections 2.1. and 2.2. are not independent. In fact, the following

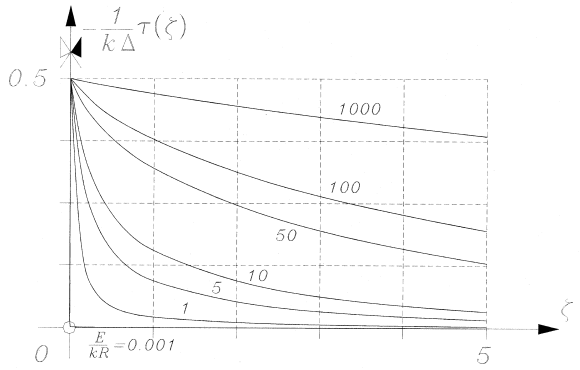

Fig. 8. The interface stress $\tau(\zeta)$ for the glass-epoxy composite.

relations hold:

$$\tau(\zeta) = -E\pi R\frac{\Delta}{P}\frac{\mathrm{d}\tau_{\mathrm{cf}}(\zeta)}{\mathrm{d}\zeta}, \tag{20a}$$

$$u(\zeta) = -E\pi R\frac{\Delta}{P}\frac{\mathrm{d}u_{\mathrm{cf}}(\zeta)}{\mathrm{d}\zeta}, \tag{20b}$$

$$U(\zeta) = -\frac{\Delta}{P}N_{\mathrm{cf}}(\zeta), \tag{20c}$$

$$N(\zeta) = 2E\pi^2R^3\frac{\Delta}{P}\tau_{\mathrm{cf}}(\zeta), \tag{20d}$$

$$\tau_{\mathrm{rr}}(\zeta) = -E\pi R\frac{\Delta}{P}\frac{\mathrm{d}\tau_{\mathrm{rr,\ cf}}(\zeta)}{\mathrm{d}\zeta}, \tag{20e}$$

$$\tau_{\mathrm{zz}}(\zeta) = -E\pi R\frac{\Delta}{P}\frac{\mathrm{d}\tau_{\mathrm{zz,\ cf}}(\zeta)}{\mathrm{d}\zeta}, \tag{20f}$$

where $\tau_{\mathrm{cf}}(\zeta)$, $u_{\mathrm{cf}}(\zeta)$, $N_{\mathrm{cf}}(\zeta)$, $\tau_{\mathrm{rr,cf}}(\zeta)$ and $\tau_{\mathrm{zz,cf}}(\zeta)$ denote the quantities related to the problem of concentrated force applied to the fiber (section 2.1.). The relations (20) are a consequence of the fact that the known term in Eq. (10) is $-\mathrm{d}\epsilon^*(z)/\mathrm{d}z+f(z)/E$, and therefore to apply $\epsilon^*(z)$ is equivalent to apply the fictitious force $f(z)=-E\ \mathrm{d}\epsilon^*(z)/\mathrm{d}z$. Thus, we may use Eq. (20) and the numerical examples of section 2.1. to obtain the solutions of the present problem for the glass-epoxy composite.

Eq. (20e and f) and the figures of section 2.1. show that both the radial and longitudinal normal stresses $\tau_{\mathrm{rr}}(\zeta)$ and $\tau_{\mathrm{zz}}(\zeta)$ are even functions and change sign in the positive ζ-axis for $\zeta=\hat{\zeta}(k)$. The radial stress is initially a compression, and becomes a tension only for large ζ. Thus, normal interface debonding cannot occur at the fiber breaking point. The longitudinal normal stress, on the other hand, is tension for $\zeta<\hat{\zeta}(k)$ and compression for $\zeta>\hat{\zeta}(k)$. Furthermore, both $\tau_{\mathrm{rr}}(\zeta)$ and $\tau_{\mathrm{zz}}(\zeta)$ become (logarithmically) unbounded for $\zeta\to 0$ (see Eq. (19d and e)). In particular, the unboundedness of $\tau_{\mathrm{zz}}(\zeta)$ (and the fact that it is positive for $\zeta\to 0$) shows that the crack of the fiber may propagate within the matrix. This phenomenon, which has been studied, e.g. by Case et al. (1995), adds to the other well-known damage mechanism consisting in fiber-matrix sliding delamination, which has been investigated, for example, by Mbanefo and Westmann (1990).

To calculate the length of the zone of influence and to obtain the solution in terms of $\tilde{\epsilon}$, we must compute the axial force in the bar, which is given by (see Eqs. (20d) and (16a))

$$N(\zeta) = -2ER\Delta\int_0^\infty \frac{\cos(\xi\zeta)}{\dfrac{E}{kR}\xi^2 - \dfrac{E}{\mu}\xi^2 g(\xi)+2}\,\mathrm{d}\xi. \tag{21}$$

The semi-length $\bar{\zeta}$ of the zone of influence is obtained by solving $N(\bar{\zeta})=0.05\mathrm{N}(0)$ and it is illustrated in Fig. 7(b). Qualitatively, it has the same behavior as the corresponding curve for the concentrated force, apart from the fact that it is much more inclined, showing a stronger dependence of the zone of influence on the interface stiffness.

Finally, by using Eq. (21) we can easily compute the function $\Delta = \Delta(\tilde{\epsilon})$ that gives the solution in terms of the applied strain $\tilde{\epsilon}$:

$$\Delta = \tilde{\epsilon}\frac{\pi R}{2}\frac{1}{\displaystyle\int_0^\infty \frac{\mathrm{d}\xi}{\dfrac{E}{kR}\xi^2 - \dfrac{E}{\mu}\xi^2 g(\xi) + 2}}. \tag{22}$$

It follows that the actual axial force in the bar is given by

$$\tilde{N}(\zeta) = \tilde{\epsilon}E\pi R^2 \frac{\displaystyle\int_0^\infty \frac{[1-\cos(\xi\zeta)]\,\mathrm{d}\xi}{\dfrac{E}{kR}\xi^2 - \dfrac{E}{\mu}\xi^2 g(\xi) + 2}}{\displaystyle\int_0^\infty \frac{\mathrm{d}\xi}{\dfrac{E}{kR}\xi^2 - \dfrac{E}{\mu}\xi^2 g(\xi) + 2}} = \tilde{\epsilon}E\pi R^2\left[1 - \frac{\tau_{\mathrm{cf}}(\zeta)}{\tau_{\mathrm{cf}}(0)}\right]. \tag{23}$$

3. The cylinder model

The dilute concentration hypothesis previously employed is no longer acceptable when there are many fibers embedded in the matrix. In this case, the reciprocal interactions between neighboring fibers cannot be neglected, and we need an improved model to describe the mechanical behavior of the composite. The density of the fiber is commonly measured by the volume fraction

$$V_{\mathrm{f}} = \frac{\mathrm{vol(fibre)}}{\mathrm{vol(fibre)} + \mathrm{vol(matrix)}}. \tag{24}$$

In practical applications it is frequent to have $V_{\mathrm{f}} = 0.65 \div 0.75$, which is very near to the maximum theoretical density $V_{\mathrm{f}} \cong 0.907$ obtained for triangular packing of touching fibers.

The microscopical characterization of the composite is not possible, because experiments show a great complexity in the distribution of the fiber within the matrix (Subramanian et al., 1996). To overcome

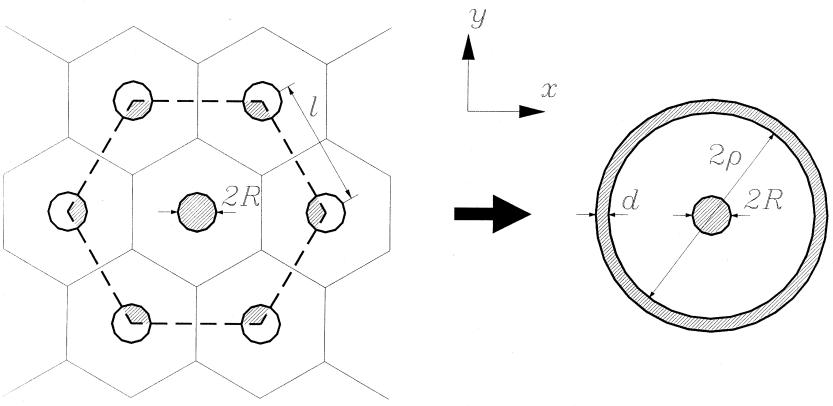

Fig. 9. The hexagonal arrays of fibers and the cylinder model.

this difficulty, we suppose a *statistically homogeneous* (Hashin, 1983) behavior of the material, namely, the composite behaves like an *ordered* one with the same V_f. The simplest ordered distributions are those with square or hexagonal (Fig. 9) arrays of fibers. The latter, in particular, is often preferred because it maintains the transversal isotropy and because it shows a better agreement with experiments.

We have simplified the problem to that of the hexagonal cell periodically repeated. However, in this form the problem cannot be solved analytically, and another commonly used simplification is required. We approximate the six neighboring fibers (around the considered one) by a concentric annular ring made of the same material (Fig. 9). The external ring is linked to the central fiber by another annular ring made of the same material as the matrix. This approximation is known as the *cylinder model*, and it is widely used in the literature of composites (see, for example, Tandon, 1995 and Case et al., 1995). It should be noted that this model neglects the interactions with distant fibers and the non-uniformity with respect to the angular variable θ.

As suggested by Tandon (1995), there are two different approaches allowing for the determination of the cylinder model free parameters ρ (the radius of the matrix ring) and d (the width of the external ring) in terms of micro-mechanical parameters R and V_f of the original composite. In both cases it is assumed that the external ring has the same area as the (part) of the six fibers related to the central one (see Fig. 9), namely, $6 \times (1/3) \times \pi R^2 = 2\pi R^2$. This leads to the first equation

$$2R^2 = 2\rho d + d^2. \tag{25}$$

The two approaches differ for the second equation to be added to Eq. (25). In the first case, the same fibers distance is assumed in the model and in the hexagonal array, namely, $\rho = l - R$. Being $R/l = \sqrt{V_f \sqrt{3}/(2\pi)}$, we have therefore, after some simplifications,

$$\frac{\rho}{R} = \sqrt{\frac{2\pi}{V_f\sqrt{3}}} - 1, \tag{26a}$$

$$\frac{d}{R} = 1 - \sqrt{\frac{2\pi}{V_f\sqrt{3}}} + \sqrt{\frac{2\pi}{V_f\sqrt{3}} - 2\sqrt{\frac{2\pi}{V_f\sqrt{3}}} + 3}. \tag{26b}$$

In the second case, on the other hand, it is assumed that the cylinder model has the same density V_f as the original composite. This gives

$$\rho = \sqrt{\frac{3\sqrt{3}}{2\pi} l^2 - 2R^2}, \tag{27}$$

which, added to Eq. (25), furnishes

$$\frac{\rho}{R} = \sqrt{\frac{3}{V_f} - 2}, \tag{28a}$$

$$\frac{d}{R} = \sqrt{\frac{3}{V_f}} - \sqrt{\frac{3}{V_f} - 2}. \tag{28b}$$

The difference between Eqs. (26) and (28) is about 10% on average, and therefore it is not negligible. We guess that Eq. (26) is better for higher values of V_f, while for lower values of V_f the expression (28)

should be preferable. However, the best way to choose between the two models is the comparison between experiments.

We continue to use the Mbanefo and Westmann hypothesis both for the central fiber and for the external ring. To simplify the exposition, we denote with $U_1(z)$ and $U_2(z)$, respectively, their longitudinal displacements, and we define $u_1(z)=u_z(R,z)$ and $u_2(z)=u_z(\rho, z)$. The interface stresses, on the other hand, are denoted by $\tau_1(z)$ and $\tau_2(z)$.

The Love potential function in the matrix is given by Eq. (5). The boundary conditions $u_r(R, z)=0$ and $u_r(\rho, z)=0$ make it possible to obtain two of the four unknowns $A(s)$, $B(s)$, $C(s)$ and $D(s)$ in terms of the others:

$$A(s) = B(s)\frac{|s|RK_0(|s|R)I_1(|s|\rho) - |s|\rho K_0(|s|\rho)I_1(|s|R)}{I_1(|s|R)K_1(|s|\rho) - I_1(|s|\rho)K_1(|s|R)} + D(s)\frac{-|s|RI_0(|s|R)I_1(|s|\rho) + |s|\rho I_0(|s|\rho)I_1(|s|R)}{I_1(|s|R)K_1(|s|\rho) - I_1(|s|\rho)K_1(|s|R)}, \tag{29a}$$

$$C(s) = B(s)\frac{|s|RK_0(|s|R)K_1(|s|\rho) - |s|\rho K_0(|s|\rho)K_1(|s|R)}{I_1(|s|R)K_1(|s|\rho) - I_1(|s|\rho)K_1(|s|R)} + D(s)\frac{-|s|RI_0(|s|R)K_1(|s|\rho) + |s|\rho I_0(|s|\rho)K_1(|s|R)}{I_1(|s|R)K_1(|s|\rho) - I_1(|s|\rho)K_1(|s|R)}. \tag{29b}$$

Substituting Eq. (29) in Eq. (4) we obtain $\hat{u}_1(s)$, $\hat{u}_2(s)$, $\hat{\tau}_1(s)$ and $\hat{\tau}_2(s)$ in terms of $B(s)$ and $D(s)$. Rearranging, one arrives at the relation between $\hat{u}_1(s)$, $\hat{u}_2(s)$ and $\hat{\tau}_1(s)$, $\hat{\tau}_2(s)$:

$$\hat{u}_1(s) = \frac{R}{\mu}\{\hat{\tau}_1(s)\alpha(|s|R, |s|\rho) + \hat{\tau}_2(s)\beta(|s|R, |s|\rho)\}, \tag{30a}$$

$$\hat{u}_2(s) = \frac{\rho}{\mu}\{\hat{\tau}_1(s)\beta(|s|\rho, |s|R) + \hat{\tau}_2(s)\alpha(|s|\rho, |s|R)\}, \tag{30b}$$

where the two unsymmetrical functions $\alpha(x, y)$ and $\beta(x, y)$ are defined as

$$\alpha(x, y) = \frac{1}{4(1-\nu)} - \frac{1}{x}\frac{K_0(x)I_1(y) + I_0(x)K_1(y)}{K_1(x)I_1(y) - K_1(y)I_1(x)} + \frac{\frac{1}{x^2} - [K_0(x)I_1(y) + I_0(x)K_1(y)]^2}{4(1-\nu)[K_1(x)I_1(y) - K_1(y)I_1(x)]^2}, \tag{31a}$$

$$\beta(x, y) = \frac{1}{x^2}\frac{1}{K_1(x)I_1(y) - K_1(y)I_1(x)} + \frac{\frac{1}{x}[K_0(x)I_1(y) + I_0(x)K_1(y)] - \frac{y}{x^2}[K_0(y)I_1(x) + I_0(y)K_1(x)]}{4(1-\nu)[K_1(x)I_1(y) - K_1(y)I_1(x)]^2}, \quad x, y > 0. \tag{31b}$$

In the cylinder model, the external ring is not loaded and therefore its equilibrium equation is given by

$$\frac{d^2U_2(z)}{dz^2} - \frac{\rho}{ER^2}\tau_2(z) = 0, \tag{32}$$

or, in the Fourier transform space,

$$-s^2\hat{U}_2(s) - \frac{\rho}{ER^2}\hat{\tau}_2(s) = 0. \tag{33}$$

At the external interface $r=\rho$, the stress and the displacements verify the interface condition $\hat{\tau}_2(s) = k_2[\hat{U}_2(s) - \hat{u}_2(s)]$, where k_2 is the stiffness of the external interface, which may be different from k_1, the stiffness of the internal interface. Substituting this equation in Eq. (33) we obtain

$$\hat{u}_2(s) = -\hat{\tau}_2(s)\left[\frac{1}{k_2} + \frac{\rho}{ER^2}\,\frac{1}{s^2}\right], \tag{34}$$

and successively, by using Eq. (30b),

$$\hat{\tau}_1(s)\beta(|\,s\,|\,\rho, |\,s\,|\,R) = -\hat{\tau}_2(s)\left[\alpha(|\,s\,|\,\rho, |\,s\,|\,R) + \frac{\mu}{\rho k_2} + \frac{\mu}{ER^2}\,\frac{1}{s^2}\right]. \tag{35}$$

Substituting from Eq. (35) in Eq. (30a) we finally obtain the equivalent of Eq. (8) for this problem:

$$\hat{u}_1(s) = \hat{\tau}_1(s)\frac{R}{\mu}g_{\mathrm{cyl}}\left(|\,s\,|\,R; \frac{\rho}{R}, \frac{\mu}{E}, \frac{\mu}{\rho k_2}\right), \tag{36}$$

where

$$g_{\mathrm{cyl}}\left(x; \frac{\rho}{R}, \frac{\mu}{E}, \frac{\mu}{\rho k_2}\right) = \alpha\left(x, x\frac{\rho}{R}\right) - \frac{\beta\left(x, x\frac{\rho}{R}\right)\beta\left(x\frac{\rho}{R}, x\right)}{\alpha\left(x\frac{\rho}{R}, x\right) + \frac{\mu}{E}\,\frac{1}{x^2} + \frac{\mu}{\rho k_2}}, \quad x > 0. \tag{37}$$

The equilibrium equation and the interface condition for the central fiber remain unchanged with respect to the case of a single fiber (see Eqs. (11) and (2b)). It follows that the solution of the case considered in this section is simply obtained by replacing $g(x)$ with $g_{\mathrm{cyl}}(x)$ and k with k_1 in Eqs. (13)–(15), or in Eq. (16) for the case of a fiber loaded by a concentrated force or in Eq. (19) for a broken fiber. Thus, the solution of different fiber-reinforced models can be obtained simply by changing the function $g(x)$ appearing in the 'basic' expressions of the solution. It follows that this function describes (and summarizes) the mechanical properties of the composite. Furthermore, the different cases have the

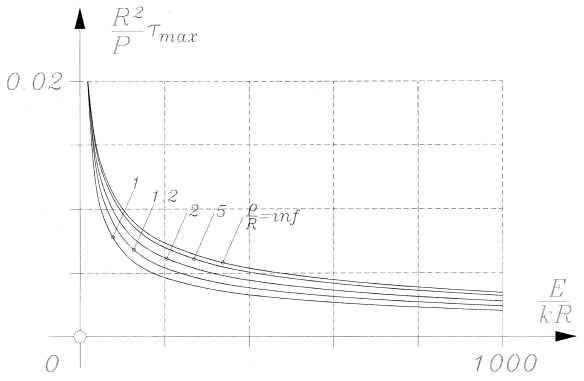

Fig. 10. The function $\tau_{\max}(k)$ for different values of the ratio ρ/R.

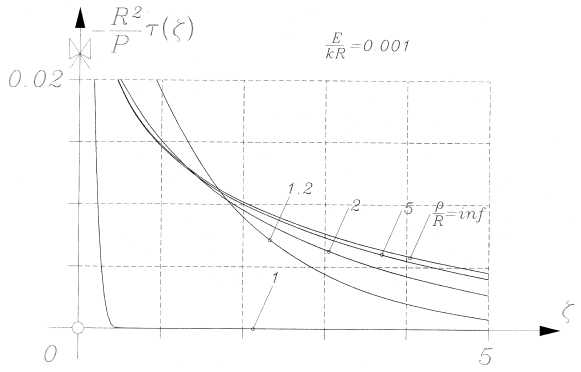

Fig. 11. The function $\tau(\zeta)$ for $E/(kR)=0.001$ and for different values of ρ/R.

same mathematical structure, so that, roughly speaking, they have qualitatively the same properties and the main differences should be only quantitative.

To illustrate the effect of the neighboring fibers, we have reported in Fig. 10 the maximum interface shear in the case of the concentrated force applied to the fiber (see Eq. (17)) for a glass-epoxy composite with $k_1=k_2=k$. Fig. 10 shows that for, say, $E/(kR) > 5$, the neighboring fiber relaxes the maximum interface stress, which halves on average passing from the two limit cases. For the opposite case, say for $E/(kR) < 5$, the maximum interface stress is increased, although this is not well recognizable in Fig. 10 due to graphical approximations. Thus, the effect of neighboring fibers strongly depends on the interface stiffness. In any case, we note that for approximately $\rho/R > 10$ (and for every value of $E/(kR)$) the neighboring fibers have no practical influence on the interface stress.

For the same material and load as those of Fig. 2 and for different values of k and ρ, Figs. 11–14 show the redistribution of the $\tau(\zeta)$ along the interface. The previously observed strong dependence of the interface stress on ρ and k is again highlighted by comparison of Figs. 11 and 12 (large values of k) with Figs. 13 and 14 (low values of k). In the latter case, in the initial window $0 < \zeta < 5$, $-\tau(\zeta)$ increases monotically with ρ and in the first approximation we have $\tau(\zeta, \rho_1)/\tau(\zeta, \rho_2) \cong \tau_{\max}(\rho_1)/\tau_{\max}(\rho_2)$, i.e. the knowledge of $\tau_{\max}(\rho)$ (Fig. 10) and $\tau(\zeta, \rho \to \infty)$ (Fig. 3) permits to determine $\tau(\zeta, \rho)$ for 'every' ρ. This property, however, cannot hold for every ζ, because the equilibrium relation $P = 4\pi R^2 \int_0^\infty \tau(\zeta)\, d\zeta$ and the monotony and positivity of the curves $-\tau(\zeta)$ show that the inequality $-\tau(\zeta, \rho_1) < [-\tau(\zeta, \rho_2)]$, $\rho_2 < \rho_1$, must be satisfied at least for some ζ sufficiently large.

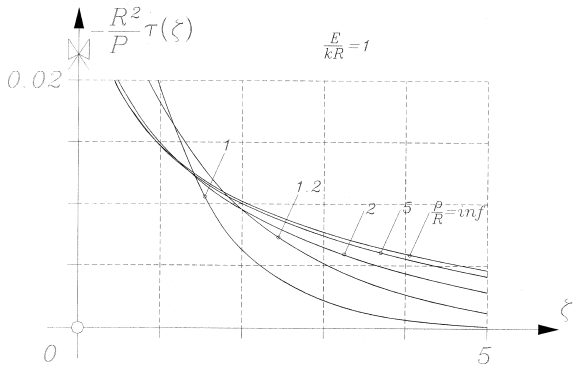

Fig. 12. The function $\tau(\zeta)$ for $E/(kR)=1$ and for different values of ρ/R.

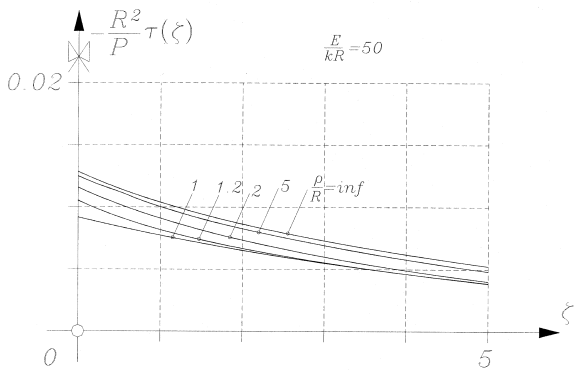

Fig. 13. The function $\tau(\zeta)$ for $E/(kR)=50$ and for different values of ρ/R.

A different situation occurs in the case of Figs. 11 and 12. In these circumstances, in fact, the non-monotonic character of the $\tau(\zeta)$ with respect to ρ is directly observable in the initial window $0 < \zeta < 5$. According to Fig. 10, we have that $-\tau(0, \rho_1) < [-\tau(0, \rho_2)]$ for $\rho_2 < \rho_1$, i.e. the maximum shear is inversely proportional to ρ. This characteristic reverts for large values of ζ. For example, in the cases of Figs. 11 and 12, the functions $-\tau(\zeta)$ are increasing with ρ for $\zeta > 2$.

Summarizing the previous observations, we have seen that the functions $-\tau(\zeta)$ are monotonically increasing with respect to ρ for (i) large k and large ζ and (ii) low k and low ζ, monotonically decreasing in the other cases.

4. The shear lag model

The *shear lag* model (Cox, 1952) is a simplification of the cylinder model which consists in assuming that the matrix has only constant shear deformation in the radial direction. This model is characterized by the relation

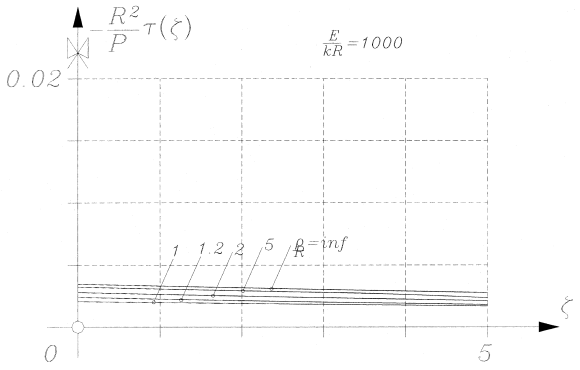

Fig. 14. The function $\tau(\zeta)$ for $E/(kR)=1000$ and for different values of ρ/R.

$$\tau_1(z) = \mu \frac{u_2(z) - u_1(z)}{\rho - R}. \tag{38}$$

It is worth remarking that Eq. (38) shows that the matrix actually behaves like a weak interface of stiffness $\mu/(\rho - R)$.

In the present case the solution can be easily obtained in the physical space. For example, the interface tangential stress in the case of concentrated force applied to the fiber is given by

$$\tau(\zeta) = -\frac{P}{R^2} \frac{\sqrt{3/a}}{6\pi} \mathrm{e}^{-|\zeta|\sqrt{3/a}}, \tag{39a}$$

where

$$a = \frac{E}{k_1 R} + \frac{E}{\mu}\left(\frac{\rho}{R} - 1\right) + \frac{E}{\rho k_2}. \tag{39b}$$

However, in order to make a comparison between the cases treated in sections 2 and 3, we prefer to look for the solution in the Fourier transform space. Indeed, using the equilibrium and external interface equations we arrive at

$$\hat{u}_1(s) = \hat{\tau}_1(s) \frac{R}{\mu} g_{\mathrm{sl}}\left(\mid s \mid R; \frac{\rho}{R}, \frac{\mu}{E}, \frac{\mu}{\rho k_2} \right), \tag{40}$$

where

$$g_{\mathrm{sl}}\left(x; \frac{\rho}{R}, \frac{\mu}{E}, \frac{\mu}{\rho k_2} \right) = 1 - \frac{\rho}{R} - \frac{\mu}{\rho k_2} - \frac{\mu}{E} \frac{1}{x^2}. \tag{41}$$

Again the solution is obtained by replacing $g(x)$ with $g_{\mathrm{sl}}(x)$ and k with k_1 in Eqs. (13)–(15), or in Eq. (16) for that case of fiber loaded by a concentrated force and in Eq. (19) for a broken fiber.

5. The limit cases of the cylinder model

In the cylinder model, when ρ increases (i.e. when V_{f} decreases) the interaction between the fibers decreases, and when ρ tends to infinity (V_{f} tends to zero), the dilute concentration hypothesis should be exact. On the other hand, when the fibers are very close to each other, the 'width' of the matrix is low and the shear tends to become constant, i.e. the shear lag model should be a good approximation in this case. To mathematically justify these heuristic considerations, we must prove that the following two limits hold:

$$\lim_{\rho \to R} g_{\mathrm{cyl}}\left(x; \frac{\rho}{R}, \frac{\mu}{E}, \frac{\mu}{\rho k_2} \right) = g(x), \tag{42a}$$

$$\lim_{\rho \to R} g_{\mathrm{cyl}}\left(x; \frac{\rho}{R}, \frac{\mu}{E}, \frac{\mu}{\rho k_2} \right) = \lim_{\rho \to R} g_{\mathrm{sl}}\left(x; \frac{\rho}{R}, \frac{\mu}{E}, \frac{\mu}{\rho k_2} \right) = -\frac{\mu}{E} \frac{1}{x^2} - \frac{\mu}{R k_2}. \tag{42b}$$

To prove the first limit, we note that for $x \to \infty$ the Bessel functions admit the asymptotic developments (Abramowitz and Stegun, 1970, section 9.7)

$$K_0(x) \cong K_1(x) \cong \mathrm{e}^{-x}\sqrt{\frac{\pi}{2x}} + \cdots, \tag{43a}$$

$$I_0(x) \cong I_1(x) \cong \frac{\mathrm{e}^{x}}{\sqrt{2\pi x}} + \cdots, \tag{43b}$$

which implies that

$$\lim_{y\to\infty} \alpha(x, y) = g(x), \qquad \lim_{y\to\infty} \alpha(y, x) = 0, \tag{44a}$$

$$\lim_{y\to\infty} \beta(x, y) = 0, \qquad \lim_{y\to\infty} \beta(y, x) = 0. \tag{44b}$$

Eq. (44) proves the first limit (42a). To compute the second limit, on the other hand, we note that, for $\rho \to R$,

$$\alpha\left(x, x\frac{\rho}{R}\right) \cong -\alpha\left(x\frac{\rho}{R}, x\right) \cong -\beta\left(x, x\frac{\rho}{R}\right) \cong \beta\left(x\frac{\rho}{R}, x\right) \cong$$

$$\cong \left(1 - \frac{1}{2(1-\nu)}\right)\frac{1}{x^2(1-\rho/R)} + \cdots = \frac{b}{1-\rho/R} + \cdots, \tag{45}$$

where the relation $K_0(x)I_1(x) + K_1(x)I_0(x) = 1/x$ has been employed. Substituting from Eq. (45) into Eq. (37) we obtain, for $\rho \to R$,

$$g_{\mathrm{cil}}\left(x; \frac{\rho}{R}, \frac{\mu}{E}, \frac{\mu}{\rho k_2}\right) \cong \frac{b}{1-\rho/R} - \frac{-\left(\dfrac{b}{1-\rho/R}\right)^2}{-\dfrac{b}{1-\rho/R} + \dfrac{\mu}{E}\dfrac{1}{x^2} + \dfrac{\mu}{Rk_2}} + \cdots \cong -\frac{\mu}{E}\frac{1}{x^2} - \frac{\mu}{Rk_2} + \cdots. \tag{46}$$

6. Conclusions

The influence of the interface stiffness in the diffusion of load from a fiber to a surrounding matrix has been analyzed. It has been shown that, contrarily to the classical case of perfect bonding, the weak interface avoids stress singularities and permits a better redistribution of the tangential interface stress. In particular, it increases the length of the zone of influence.

The general solution has been obtained in closed form, and the cases of single force applied to the fiber and of broken fiber have been investigated in detail. In both cases, the analytical results are discussed and illustrated by means of numerical examples. Three different models have been considered: the dilute concentration hypothesis (no interaction between fibers), the cylinder model and the shear lag model (low distance between neighboring fibers or, equivalently, high values of the volume fraction V_{f}). In both cases, the problems have the same governing equations, and the solutions of one problem can be obtained on the basis of the solution of another problem by a simple shrewd substitution of a given function appearing in the expression of the solution. Furthermore, it has been shown that the dilute concentration and the shear lag are the two (opposite) limit cases of the cylinder model when the distance between the fiber becomes infinite and vanishes, respectively.

Acknowledgements

The work of S.L. has been supported by European Community under the program Training and Mobility of Researchers (TMR), contract ERBFMBI CT97 2458. This financial support is greatly acknowledged.

References

Abramowitz, M., Stegun, I.A., 1970. Handbook of Mathematical Functions. Dover Publications, New York.
Achenbach, J.D., Zhu, H., 1989. Effect of interfacial zone on mechanical behavior and failure of fiber-reinforced composites. J. Mech. Phys. Solids 37 (3), 381–393.
Achenbach, J.D., Zhu, H., 1990. Effect of interphases on micro and macromechanical behavior of hexagonal-array fiber composites. J. Appl. Mech. 57, 956–963.
Benscoter, S., 1949. Analysis of a single stiffener on an infinite sheet. J. Appl. Mech. 16, 242–246.
Benveniste, Y., 1985. The effective mechancial behavior of composite materials with imperfect contact between the constituents. Mechanics of Material 4, 197–208.
Case, S.W., Carman, G.P., Lesko, J.J., Fajardo, A.B., Reifsnider, K.L., 1995. Fiber fracture in unidirectional composites. J. Comp. Mater. 29 (2), 208–228.
Choi, H.S., Achenbach, J.D., 1995. Stress states at neighboring fibers induced by single-fiber interphase defects. Int. J. Solids Structures 32 (11), 1555–1570.
Cox, H.L., 1952. The elasticity and strength of a paper and other fibrous materials. British Journal of Applied Physics 3, 72–79.
Devries, F., 1993. Bounds on elastic moduli of unidirectional composites with imperfect bonding. Composites Engineering 3 (4), 349–382.
Erdogan, F., Gupta, G.D., 1971. The problem of an elastic stiffener bonded to a half plane. J. Appl. Mech. 38, 937–941.
Ford, E.F., 1973. Stress analysis of a broken fiber imbedded in an elastic medium, D.E.A.P. Harvard University, Tech. Report n. 1.
Geymonat, G., Krasucki, F., Lenci, S., 1999. Mathematical analysis of a bonded joint with a soft thin adhesive, Math. Mech. Solids 4, 201–225.
Goodier, J.N., Hsu, C.S., 1954. Trasmission of tension from a bar to a plate. J. Appl. Mech. 21, 147–150.
Grigolyuk, E.I., Tolkachev, V.M., 1987. Contact Problems in the Theory of Plates and Shells. Mir Publisher, Moscow.
Hashin, Z., 1983. Analysis of composite materials—a survey. J. Appl. Mech. 50, 481–505.
Hashin, Z., 1990. Thermoelastic properties of fiber composites with imperfect interface. Mech. Mater. 8, 333–348.
Hashin, Z., 1991. Thermoelastic properties of particulate composites with imperfect interface. J. Mech. Phys. Solids 39, 745–762.
Hull, D., 1981. An Introduction to Composite Materials. Cambridge University Press, Cambrige.
Koiter, W.T., 1955. On the diffusion of load from a stiffener into a sheet. Quart. J. Mech. App. Math. VIII, 164–178.
Lee, V-G., Mura, T., 1994a. Load diffusion and absorption problems from a finite fiber to elastic infinite matrix. J. Appl. Mech. 61, 567–574.
Lee, V-G., Mura, T., 1994b. Load transfer from a finite cylindrical fiber into an elastic half-space. J. Appl. Mech. 61, 971–975.
Lene, F., Leguillon, D., 1982. Homogenized constitutive law for a partially cohesive composite material. Int. J. Solids Struct. 18, 443–458.
Love, A.E.H., 1926. A Treatise on the Mathematical Theory of Elasticity, Oxford, reprint Dover Publications, New York, 1944.
Mbanefo, U., Westmann, R.A., 1990. Axisymmetric stress analysis of a broken, debonded fiber. J. Appl. Mech. 57, 654–660.
Melan, E., 1932. Ein beitrag zur theori geschweisster verbindungen. Ingenier-Archiv 3, 123–129.
Muki, R., Sternberg, E., 1969. On the diffusion of an axial load from an infinite cylindrical bar embedded in an elastic medium. Int. J. Solids Struct. 5, 587–605.
Muki, R., Sternberg, E., 1970. Elastostatic load-transfer to a half-space from a partially embedded axially loaded rod. Int. J. Solids Struct. 6, 69–90.
Muki, R., Sternberg, E., 1971. Load-absorption by a discontinuous filament in a fiber-reinforced composite. ZAMP 22, 809–824.
Pak, R.Y.S., Saphores, J-D.M., 1991. On the response of partially embedded rod to axial load. J. Appl. Mech. 58, 599–602.
Peters, P.W.M., Martin, E., Quenisset, J.M., 1995. Slip and frictional shear stresses in ceramic composites. J. Compos. Mater. 29 (5), 550–572.
Sneddon, I.N., 1951. Fourier Transforms. McGraw-Hill, London.
Subramanian, S., Lesko, J.J., Reifsnider, K.L., Stinchcomb, W.W., 1996. Characterization of the fiber-matrix interphase and its influence on mechanical properties of unidirectional composites. J. Comp. Mater. 30 (3), 309–332.

Tandon, G.P., 1995. Use of composite cylinder model as representative volume element for unidirectional fiber composites. J. Comp. Mater. 29 (3), 388–409.
Weitsman, Y., Zhu, H., 1993. Multi-fracture of ceramic composites. J. Mech. Phys. Solids 41 (2), 351–388.